Growth sequence and interface formation in the Fe/MgO/Fe(001) tunnel junction analyzed by surface x-ray diffraction

C. Tusche,[1,*] H. L. Meyerheim,[1] N. Jedrecy,[2] G. Renaud,[3] and J. Kirschner[1]
[1]*Max-Planck-Institut für Mikrostrukturphysik, Weinberg 2, D-06120 Halle, Germany*
[2]*Institut des NanoSciences de Paris, Universités Paris 6 et 7 et CNRS-UMR 7588, 4 place Jussieu, F-75252 Paris Cedex 05, France*
[3]*CEA-Grenoble, 17 rue des Martyrs, F-38054 Grenoble, France*
(Received 2 May 2006; revised manuscript received 10 July 2006; published 16 November 2006)

We present a surface x-ray diffraction study of the interface geometric structure in the Fe/MgO/Fe(001) magnetic tunnel junction (MTJ). While the lower MgO/Fe(001) interface is characterized by a substoichiometric FeO_x ($x=0.6\pm0.1$) layer in agreement with previous studies, growth of Fe on the MgO spacer and the upper Fe/MgO interface structure strongly depends on the preparation method. If 0.4 monolayers of Fe are initially deposited in ambient oxygen atmosphere ($p=10^{-7}$ mbar) followed by Fe deposition under ultrahigh-vacuum (UHV) conditions, structural coherence across the trilayer junction is observed. In this case, substoichiometric FeO_x layers are present at both Fe/MgO interfaces corresponding to a symmetric MTJ structure. In contrast, lattice registry is not preserved if Fe deposition is carried out solely under UHV conditions. Our results might have important implications for the preparation of magnetic tunnel junctions optimized to achieve giant tunneling-magnetoresistance amplitudes.

DOI: 10.1103/PhysRevB.74.195422 PACS number(s): 68.35.Ct, 61.10.−i, 75.70.Ak

I. INTRODUCTION

When the magnetization-dependent tunneling of electrons through an insulating barrier sandwiched between two ferromagnetic electrodes was first reported in 1975 by Julliere,[1] the change of the resistance was solely related to the spin polarization of the two electrodes, i.e., the ratio between the numbers of minority and majority electrons at the interface. In general, the magnitude of the effect is defined by the tunneling magnetoresistance ratio (TMR) $(R_{AP}-R_P)/R_P$, where R_P and R_{AP} represent the resistance for parallel and antiparallel alignment of the electrodes, respectively.

Efforts in improving the TMR amplitude go in parallel with the continuously increasing technological relevance of TMR multilayer systems in information technology. Magnetic tunnel junctions (MTJs) not only play a role in data storage systems as readheads for hard drives or nonvolatile memory cells in magnetic random access memories, but also in the developing field of spintronics. Here, the spin degree of freedom becomes the information carrier instead of the charge.[2] In order to optimize the TMR amplitude for such applications numerous attempts to prepare MTJs were carried out.

Considerable attention has been focused on the study of MTJs involving amorphous oxide barriers like alumina (Al_2O_3). Carefully chosen electrode materials and optimized growth of the barrier have led to TMR amplitudes up to 70% at room temperature.[3] On the basis of the Julliere model, high TMR values require electrode materials characterized by a spin polarization close to 100%. Although many systems were investigated only limited success was achieved. Furthermore, due to scattering of the electrons within the amorphous barrier leading to a randomization of the parallel component of the electron momentum ($\vec{k}_\parallel$), only a limited theoretical description of the tunneling process is possible.

In order to overcome these limitations, MTJs based on monocrystalline tunneling barriers sandwiched between ferromagnetic electrodes might open the field to achieve extremely high TMR amplitudes. Tunneling is ballistic in this case, i.e., the parallel component of the electron momentum $\vec{k}_\parallel$ is conserved.[4] Large TMR values are achieved if Bloch states of different symmetry decay at different rates in the barrier.

Due to the low lattice mismatch of only 3.7% the Fe/MgO/Fe junction is widely investigated, both experimentally, and theoretically.[5–12] Tunneling in the P alignment is dominated by electronic states near $\vec{k}_\parallel=\vec{0}$ through the slowly decaying Δ_1 state in the MgO spacer, leading to a small R_P.[4] This state is not present in the AP alignment, leading to a large R_{AP}. Consequently, TMR values up to several times 1000% were theoretically predicted based on model structures assuming abrupt Fe/MgO interfaces.[4,7]

Since $\vec{k}_\parallel$ conservation is a prerequisite for achieving giant TMR amplitudes, structural perfection and lattice registry across the interfaces is mandatory, but hardly achievable and controllable. In the case of the Fe/MgO/Fe(001) junction, experimental TMR values up to 250% were reported,[12] much less than theoretically predicted. The discrepancy could in part be related to differences between the theoretically assumed and the true interface structures.

For the bottom MgO/Fe(001) interface, an interfacial FeO_x layer characterized by a substoichiometric oxygen concentration ($x=0.6\pm0.1$) was determined by surface x-ray diffraction (SXRD).[13,14] In agreement with this experimental finding, a very recent theoretical study by Yu *et al.*[15] suggests that the formation of the FeO_x-interface structure is related to the presence of excess oxygen. Experimentally, this has been observed in a previous study where MgO was deposited by evaporation from a polycrystalline MgO rod.[16] Calculations by Zhang *et al.*[8] have shown that the presence of only one FeO_x-interface layer corresponding to an asymmetric MTJ ($Fe/FeO_x/MgO/Fe$) leads to a reduction of the TMR ratio by reducing the coupling of the Δ_1 state in the MgO spacer to the Fe electronic Bloch states.[8] The decisive role of the in-

terface structure in the transport properties was also proven in recent experimental studies on resonant tunneling through interface states involving the minority-channel conductance[9] and by the observation of an asymmetric current-voltage characteristic.[10–12] The latter was tentatively attributed to asymmetric interface structures in the Fe/MgO/Fe MTJ.

A major problem in the preparation of single-crystalline Fe/MgO/Fe(001) junctions is that two-dimensional growth of metallic Fe on top of the oxide is inhibited by the larger surface free energy of Fe (2.9 J/m^2) as compared to MgO (1.1 J/m^2).[17,18] Therefore, layer-by-layer growth is favored for MgO on Fe but not vice versa. Fe starts to nucleate in three-dimensional (3D) islands which coalesce at a coverage of a few monolayers (ML), but the surface roughness cannot be removed completely.[5,6,19–21] It is tempting to speculate that 3D growth might introduce considerable structural disorder at the Fe/MgO interface, at variance with requirements for coherent tunneling.

In summary, thus far there is only limited knowledge about the structural details of the top (Fe/MgO) interface in the Fe/MgO/Fe(001) MTJ. For this reason we have carried out a thorough structure analysis of the Fe/MgO/Fe(001) trilayer using surface x-ray diffraction,[22] a well-established tool for the analysis of surface structures and buried interfaces. The growth mode of the top Fe electrode on the MgO spacer and the geometric structure at the Fe/MgO interface depend on whether Fe is initially deposited in ambient oxygen atmosphere or under ultrahigh-vacuum (UHV) conditions. Absence of oxygen leaves most of the deposited Fe in a disordered structure relative to the underlying crystal lattice, while registry is observed for oxygen-assisted Fe growth. In the latter case a symmetric MTJ structure characterized by FeO_x layers at both interfaces is observed.

II. EXPERIMENT

The experiments were carried out *in situ* at the beamline BM32 of the European Synchrotron Radiation Facility (ESRF) in Grenoble (France) using a six-circle ultrahigh-vacuum diffractometer[23] (base pressure 10^{-10} mbar). The (001) surface of the Fe single crystal ($\varnothing = 7$ mm) was prepared by cycles of Ar^+ ion sputtering followed by annealing until only traces of carbon were detected by Auger electron spectroscopy. The quality of the crystal surface was further checked by scanning tunneling microscopy (STM) experiments carried out in our home laboratory and *in situ* by transverse scans[23] over the (1 0 0.1) reflection, close to the (1 0 0) antiphase scattering position. STM images revealed terrace sizes of up to 500 nm, while a full width at half maximum of 0.07° was determined by the SXRD scans, both experiments indicating an excellent surface quality.

The MgO barrier was deposited on the Fe(001) substrate crystal from a polycrystalline rod heated by electron bombardment at a deposition rate of 0.125 ML/min. In all experiments 2.3 ML were deposited as calibrated by the intensity variation of the (1 0 0.1) reflection versus deposition time (not shown). Here and in the following we define 1 ML as one MgO unit (i.e., one Mg and one O atom) per surface unit cell, i.e., 1.21×10^{15} metal and oxygen atoms/cm^2. All

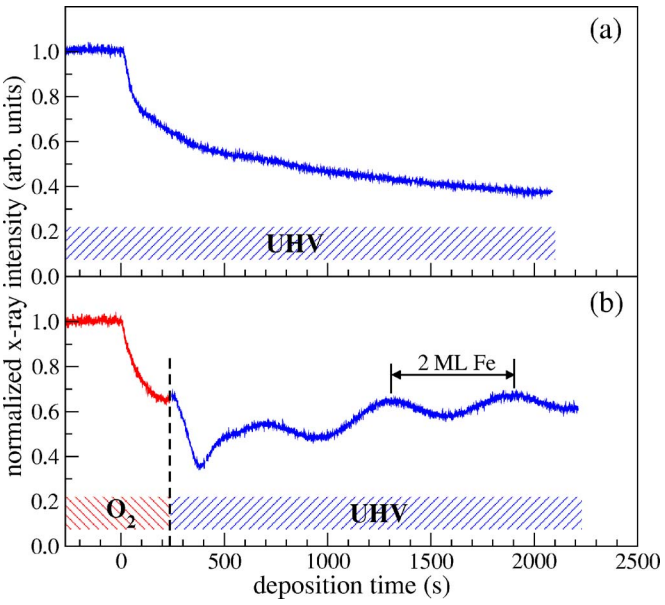

FIG. 1. (Color online) X-ray intensity at the (1 0 0.1) antiphase reflection versus deposition time for Fe on MgO/Fe(001) under UHV conditions (a) and with oxygen supplied during the growth of the first 0.4 ML (b).

depositions were carried out at room temperature. The top Fe film was deposited (deposition rate 0.22 ML/min) on the MgO layer by evaporation from a polycrystalline Fe rod heated by electron beam bombardment.[24] Two kinds of preparations were used. In the first, the upper Fe film was deposited under UHV conditions. In the second, Fe deposition was carried out under 10^{-7} mbar ambient oxygen pressure up to the first minimum of the antiphase (1 0 0.1) reflection intensity corresponding to an Fe coverage of 0.4 ML as derived by the SXRD analysis (see below). At this point the oxygen exposure was stopped and further Fe deposition was continued in UHV. In the following we refer to the growth procedures as "UHV" and "O_2" for UHV-only and oxygen-assisted deposition, respectively. Figure 1 shows the (1 0 0.1) reflection intensity versus time during deposition of the top Fe film for UHV (a) and O_2 (b) preparation. The intensity is normalized to the uncovered sample. In the experiments shown in Fig. 1 the total deposition time was about 2100 s (a) and 2230 s (b), corresponding to an Fe coverage of 7.8 and 8.3 ML, respectively.

There is clear evidence that the two preparation methods result in a different growth mode: while for Fe deposition carried out solely in UHV a continuously decreasing intensity is observed indicating increasing roughness, there is an oscillating intensity variation for oxygen-assisted growth. Note that the oxygen supply was stopped after 235 s deposition time as indicated by the vertical dashed line in Fig. 1(b), corresponding to a total Fe coverage of about 0.87 ML. This is at variance with the SXRD-derived coverage ($\approx$0.4 ML) and is related to the presence of Fe not in registry with the substrate lattice at this stage of the interface formation. During continued deposition the (1 0 0.1) intensity oscillates with a 2 ML period resulting from the in- and out-of-phase scattering contribution of subsequently growing (complete) Fe layers.

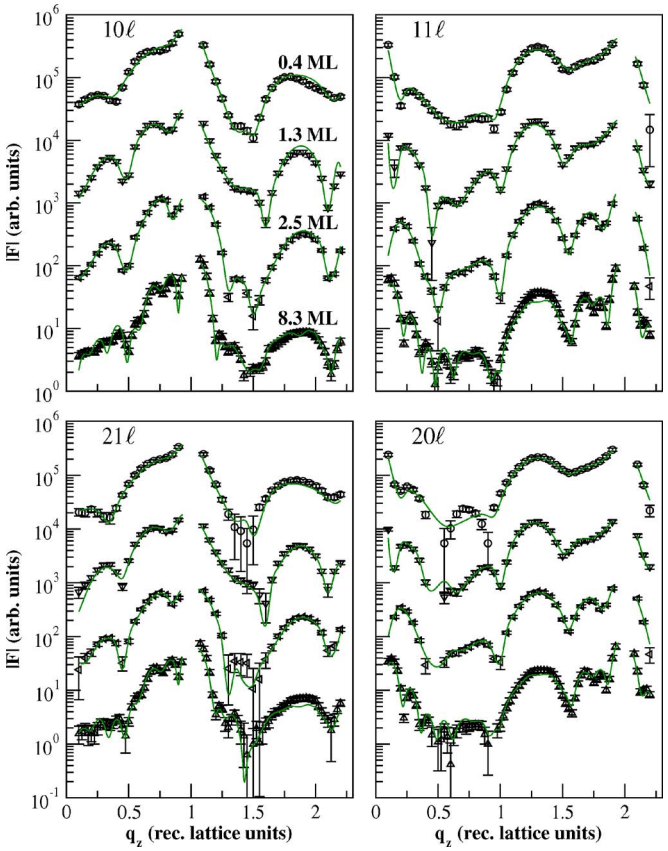

FIG. 2. (Color online) Measured (symbols) and fitted (lines) distribution of the structure factor amplitude ($|F|$) along the (1 0), (1 1), (2 0), and (2 1) crystal truncation rods for O_2 sample. Curves are shifted vertically for clarity. The total Fe coverage for the different samples is indicated at the (1 0) rods. The MgO spacer thickness is 2.3 ML in all cases.

After sample preparation integrated x-ray reflection intensities were collected at grazing incidence of the incoming beam (wavelength $\lambda=0.68$ Å) by rotating the sample around its surface normal. In total, six data sets were collected, four after O_2 growth (0.4, 1.3, 2.5, 8.3 ML) and two after UHV deposition of Fe (0.3, 7.8 ML). For each data set in total between 150 and 315 symmetry-independent reflections along four crystal truncation rods[25] (CTRs) [(1 0), (1 1), (2 0), and (2 1)] were measured up to the maximum perpendicular momentum transfer ($q_z=\ell\times c^*$) of 2.3 reciprocal lattice units (r.l.u.), equivalent to $q_z=5.04$ Å^{-1}.

While bulk reflections are characterized by integer-order reflection indices (hkl), crystal truncation leads to rods of intensity perpendicular to the surface. Therefore, the momentum transfer q_z perpendicular to the surface plane becomes a continuous parameter, while the in-plane components retain their (1×1) surface periodicity with integer h and k.[25] Bulk Bragg reflections are given by the condition: $h+k+\ell=2n$ (n integer) according to the body-centered bulk Fe lattice.

Symbols in Fig. 2 represent the structure factor amplitudes ($|F|$) along the rods for the O_2-prepared samples. They were derived after correcting the integrated intensities for geometric factors.[26]

Standard deviations (σ) derived from the counting statistics and the reproducibility of symmetry equivalent reflections[22] are represented by the error bars in Fig. 2. In general, these were found to be in the 7% range.

III. STRUCTURE MODEL FOR OXYGEN-ASSISTED GROWTH

The quantitative analysis was carried out by least-squares fit of the structure factor amplitudes calculated for a model structure to the measured ones. Solid lines in Fig. 2 represent the best fits according to the models discussed below. Almost perfect agreement between experimental and calculated structure factor amplitudes can be achieved. The fit quality is quantified by the unweighted residual (R_u).[27] We achieve $R_u=8.0\%$, 7.8%, 7.5%, and 16% for samples covered by 0.4, 1.3, 2.5, and 8.3 ML Fe, respectively. The statistically more relevant goodness of fit (GOF) parameter[27,28] lies between 1.3 and 1.6. These are excellent values, especially with respect to the complexity of the structures.

Qualitative inspection of the intensity distribution along the rods allows some general conclusions. (i) The structure factor amplitudes exhibit a pronounced modulation along q_z. This is due to the difference between the scattering contributions of the Fe and the oxide layers. The modulation frequency increases with increasing Fe overlayer thickness, qualitatively indicating coherent growth of the top Fe film. (ii) Due to the occupation of high-symmetry ($4mm$) sites within the unit cell [Fe, Mg, and O at either (0,0) and (1/2,1/2) or vice versa, alternating layer by layer], the two pairs of rods, namely, (1 0), (2 1) and (1 1), (2 0), exhibit the same overall shape, since their in-plane scattering phase given by $\exp[i2\pi(hx+ky)]$ is identical.

Since the lateral atomic positions are fixed by symmetry, only the z positions, site occupancies, and isotropic Debye parameters ($B=8\pi^2\langle u^2\rangle$, where $\langle u^2\rangle$ is the mean square displacement) need to be varied for each atomic species in a given layer. Complete Fe and MgO layers are represented by one Fe atom and by one Mg and one O atom within the surface unit cell, respectively. Occupancy factors less than 1.0 represent incomplete layers. It should be noted that no superstructures were observed in any case; therefore the lattice periodicity is always (1×1). In addition to the MgO and the top Fe electrode layers, also the two uppermost substrate Fe layers were included into the refinement. Taking account of deeper layers did not improve the fit quality.

Figure 3 shows the structure models in side view. Fe, Mg, and O atoms are represented as (blue, dark), (yellow, bright), and (large red, gray) balls, respectively. In order to clarify the layer compositions, the number of balls approximately represents the concentrations of the different species within each layer. The stoichiometry of the different phases is given within the brackets; their subscripts indicate the occupancy in percent of a monolayer. Layers are numbered from 1 (bottom) to 9 (top) as labeled on the right.

Interlayer spacings (see Table I) are listed with reference to the metal positions. Shifts of the oxygen positions out of the plane of the metal atoms in layer n are represented by the parameters δ_n (see Table II). In the following several results are summarized:

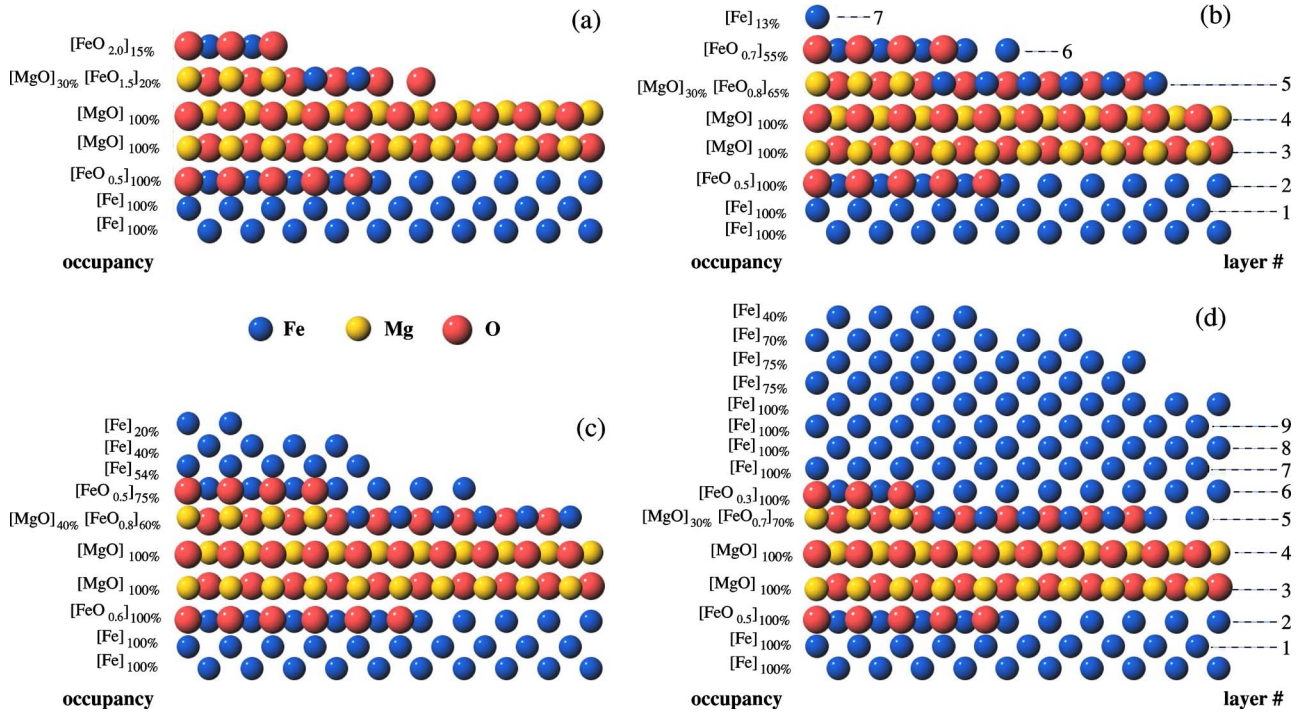

FIG. 3. (Color online) Layer-resolved model of the near-interface structure obtained by SXRD for samples grown according to O_2 method (oxygen assisted) with a total top Fe layer thickness of 0.4 (a), 1.3 (b), 2.5 (c), and 8.3 ML (d). Small dark (blue) and bright (yellow) balls represent Fe and Mg, respectively. Large (red) balls represent oxygen. The number of balls within each layer schematically represents the layer filling. Layer numbers 1–9 are shown on the right. The layer stoichiometry is given in brackets; subscripts indicate the layer filling in percent of a monolayer.

In agreement with previous studies, a substoichiometric oxide layer (FeO_x, $x \approx 0.5-0.6$) at the bottom MgO/Fe(001) interface is present in all cases (the error bar for the concentration determination is about 10% of a monolayer). The Fe atoms within the $FeO_{0.6}$ layer (2) are located 1.74 Å above the Fe-substrate layer (1; see Table I), corresponding to a 19% expansion compared to bulk Fe (d_{bulk}=1.43 Å).

Above the $FeO_{0.6}$ layer, 2.3 ML of MgO were grown in all experiments. The SXRD analysis yields a 30–40 % third-layer MgO occupation (5) above two complete MgO layers (3 and 4). Due to the lateral 3.7% compression of the MgO layer to adapt to the Fe lattice (bulk MgO lattice constant 4.21 Å versus 4.05 Å for Fe), the MgO layers are tetragonally distorted. We find large interlayer spacings up to the 2.40 Å regime corresponding to a 14% expansion relative to the bulk value of 2.105 Å. This is considerably larger than calculated by continuum elasticity theory (2.5 %), which might be related to the interaction with the FeO_x interface.

Within the experimental uncertainty the structures of all samples (O_2 and UHV) are identical as far as the MgO layer and the lower interface are concerned. In the following the evolution of the MTJ structure upon Fe deposition is discussed.

TABLE I. Layer distances d_{nm} between the metal positions of layers n and m (see also Fig. 3). Distances are given in angstroms with an error bar of about ±0.05 Å. Deeper substrate layers are fixed to the bulk layer distance of d_{Fe}=1.43 Å.

Coverage	d_{12}	d_{23}	d_{34}	d_{45}	d_{56}	d_{67}	d_{78}	d_{89}
Oxygen-assisted growth								
0.4 ML	1.74	2.30	2.35	2.24	2.16			
1.3 ML	1.67	2.27	2.32	2.30	2.28	2.23		
2.5 ML	1.72	2.27	2.31	2.39	1.89	1.53	1.35	1.50
8.3 ML	1.68	2.20	2.39	2.46	1.77	1.58	1.38	1.44
UHV-only growth								
0.3 ML	1.66	2.26	2.39	2.14	1.41			
7.8 ML	1.60	2.38	2.28	2.43	1.74	1.50	1.36	

TABLE II. Displacement (δ_n) of the oxygen atoms relative to the plane of the metal sites in layer n. Distances are given in angstroms. The error bar is estimated as ±0.10 Å. Positive values correspond to a shift toward the surface, negative ones toward the substrate.

Coverage	δ_2	δ_3	δ_4	δ_5	δ_6
Oxygen assisted growth					
0.4 ML	0.04	0.01	−0.22	−0.19	0.07
1.3 ML	0.13	0.15	−0.03	−0.11	0.04
2.5 ML	0.12	0.06	−0.12	−0.32	−0.15
8.3 ML	0.12	0.14	−0.13	−0.26	0.28
UHV-only growth					
0.3 ML	0.04	0.08	−0.18	−0.06	
7.8 ML	0.09	0.12	−0.01	−0.35	−0.41

The model in Fig. 3(a) shows the structure after deposition of 0.4 ML Fe in oxygen atmosphere. Fe atoms located in layers 5 and 6 are in an FeO-like arrangement. In both layers there seems to be some excess of oxygen as compared to the 1:1 FeO stoichiometry. However, with regard to the low total amount of Fe and oxygen we do not think that this is significant. Nevertheless it can be concluded that at this stage of the interface formation no substoichiometric $FeO_{0.6}$ phase has been formed yet.

Layer 5 also contains 0.3 ML of MgO resulting from the overdosing during MgO deposition. On the basis of the SXRD data it is not possible to distinguish whether or not MgO and FeO form a solid solution or are present as separate phases (islands). In the model presented in Fig. 3(a), FeO and MgO are represented as separate phases, since STM images have shown compact third-layer MgO islands above the complete second MgO layer,[4] and excessive site exchange processes upon Fe deposition at room temperature are not expected.

The SXRD data provide more details on the structure of the MTJ. Layer spacings for the different samples are listed in Table I. For the 0.4 ML sample, distances d_{45} and d_{56} between the oxide layers are 2.24 and 2.16 Å, respectively. These values are close to the bulk layer spacings of MgO (d_{MgO}=2.13 Å) or FeO (d_{FeO}=2.16 Å).

The z coordinates of the different metal species Fe and Mg in layer 5 were refined simultaneously using the condition z(Fe)=z(Mg). Separate refinement of the z coordinates did not improve the fit. Some possible rumpling might be reflected in an increased Debye parameter (B) determined for these atoms. We find root-mean-square displacements of $\sqrt{\langle u^2\rangle}$=0.20 Å corresponding to B=3.2 Å^2. These large values are interpreted as due to static displacements since thermal vibrations are expected to lie in the B=0.8 Å^2 range. In the Fe surface layer and within the MgO layers there is no strong enhancement relative to the bulk displacement amplitudes ($\sqrt{\langle u^2\rangle}\approx$0.10 Å). This applies to all data sets in general.

The models sketched in Figs. 3(b)–3(d) outline the evolution of the MTJ structure after subsequent Fe deposition under UHV conditions (O_2 supply stopped). In layer 5 the formation of a substoichiometric FeO_x-interface layer (x =0.7±0.1) sets in. This layer is already filled after deposition of a total amount of 1.3 ML of Fe [see Figs. 3(b) and 3(c)]. Due to the presence of 0.3 ML of MgO in layer 5, only a maximum coverage of 60–70 % of a ML can be occupied by FeO_x. The two species Fe and Mg can be separated due to their significantly different scattering amplitude, which is proportional to the atomic numbers (Z=26 versus 12 for Fe and Mg, respectively).

The comparison between the layer occupancies within the two upper oxide layers (5 and 6) in the 0.4 and 1.3 ML samples indicates an increase of the total amount of oxygen. In detail, in layers (5 and 6) the total oxygen occupancy increases from 0.6 ML (0.3+0.3) to 0.905 ML (0.520 +0.385). Similarly, the Fe coverage increases from 0.4 to 1.3 ML, i.e., by 0.9 ML while only 0.5 ML additional Fe was deposited between the experiments related to Figs. 3(a) and 3(b). We do not think that this should simply be attributed to the uncertainty of the SXRD coverage determination. Rather, we suggest that at the initial stages of the oxygen-assisted Fe deposition, some fraction of Fe and O might be present in a disordered arrangement relative to the substrate lattice, i.e., "invisible" to the CTR analysis. This conclusion is supported by the calibration of the Fe deposition rate discussed in Sec. II using Fig. 1(b). The experiment related to Fig. 3(a) was carried out after depositing Fe for 235 s corresponding to a coverage of about 0.87 ML, but only 0.4 ML are found in the CTR analysis. Moreover, adding 0.5 ML Fe results in a total coverage of 1.37 ML, now in good agreement with 1.3 ML determined from the CTR analysis [see Fig. 3(b)]. At coverages larger than 1.3 ML there is no change of the total amount of oxygen and—within the experimental uncertainty—no difference between the Fe coverage derived from the CTR analysis and the coverage determined from the deposition rate.

At Fe coverages larger than 1.3 ML, the Fe concentration in layer 6 increases. Since the oxygen occupancy in layer 6 remains constant (≈0.35) this leads to a continuously increasing Fe:O ratio in this layer ($FeO_{0.7}$, $FeO_{0.5}$, and $FeO_{0.3}$ for the 1.3, 2.5, and 8.3 ML samples, respectively). We interpret this as a continuous filling with Fe, while the fractional coverage of layer 6 by $FeO_{0.6}$ remains constant at 30–50 % of a monolayer. Simultaneously, those interlayer spacings that are involved in the changing layer composition, namely d_{56} and d_{67}, show a continuous contraction. Starting from typical values for oxides (2.2–2.3 Å) observed up to 1.3 ML they decrease to values in the 1.5–1.9 Å range for higher coverages. The latter are characteristic for (expanded) Fe spacings, very similar to the layer distance at the lower interface (d_{12}). Continued Fe deposition leads to the growth of a well-ordered top Fe film [Fig. 3(d)] characterized by interlayer distances within 5% of the bulk (bcc) Fe layer spacing.

The vertical oxygen positions were also refined. The results are summarized in Table II by the parameter δ_n representing the displacements of the oxygen atoms relative to the metal atoms in layer n. Error bars for δ_n are estimated to ±0.1 Å. The following conclusions can be made.

(i) There is some rumpling within the interfacial FeO_x layers, where oxygen in the bottom FeO_x interface (layer 2) is located above the Fe positions corresponding to a relaxation toward the MgO layer. This is in good agreement with previous SXRD results on the MgO/Fe(001) interface.[9] We also allowed for relaxations of the oxygen atoms in the first and second MgO layers. There is an upward relaxation in the first ($\delta_3>0$) and a downward relaxation in the second ($\delta_4<0$) MgO layer.

(ii) Oxygen atoms in the upper FeO_x interface (layers 5 and 6) are located below the Fe position, which again corresponds to a relaxation towards the MgO layer, making the overall structure symmetric in both composition and relaxation.

In conclusion, oxygen-assisted growth leads to a symmetric MTJ structure characterized by two FeO_x layers at the MgO/Fe interfaces and to coherent growth of the top Fe electrode.

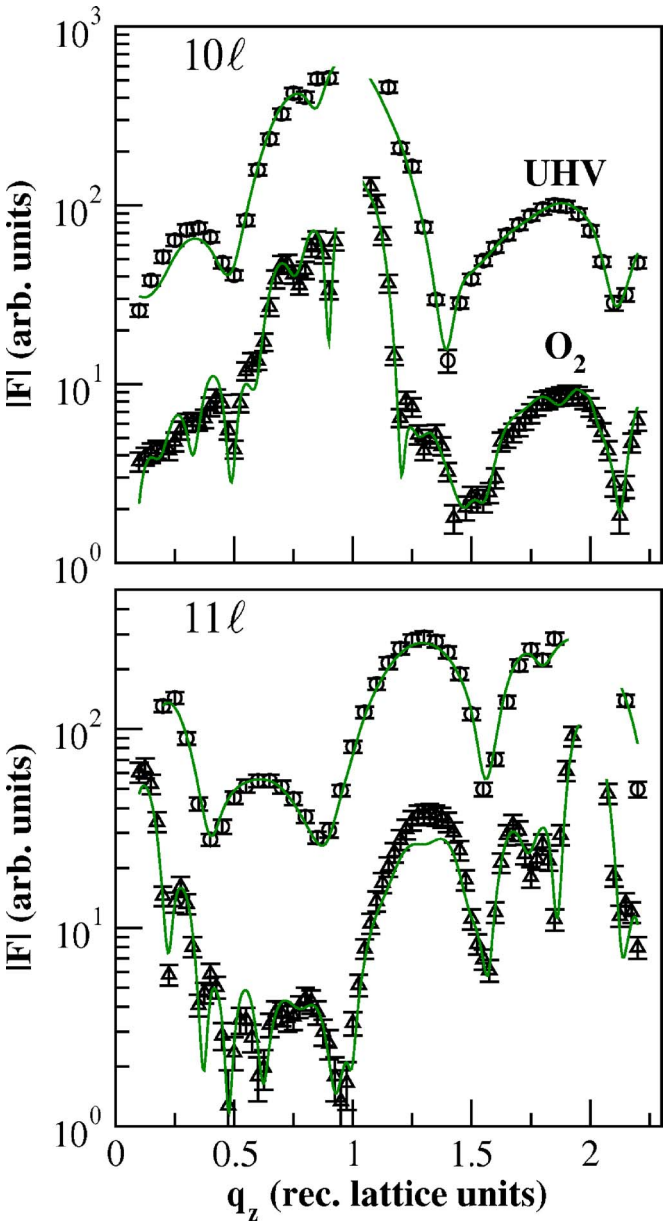

FIG. 4. (Color online) Measured (symbols) and fitted (lines) structure factor amplitudes along the (1 0) and (1 1) crystal truncation rods for 7.8 ML Fe grown in UHV (upper curves) and 8.3 ML deposited by oxygen-assisted growth (lower curves). Curves are shifted vertically for clarity.

IV. STRUCTURE MODEL FOR UHV-ONLY GROWTH

Figure 4 compares the (1 0) and the (1 1) rods measured for samples prepared by methods UHV and O_2. The total Fe coverage is about the same (7.8 and 8.3 ML) for both samples. In the case of the UHV sample the rods are considerably less structured as compared to the O_2 sample, qualitatively suggesting a reduced number of layers contributing to the scattered intensity. This is in agreement with the observations shown in Fig. 1.

The results of the structure analysis for the two UHV-prepared samples are summarized in Fig. 5 and in the lower part of Tables I and II. Direct inspection of Fig. 5 shows only

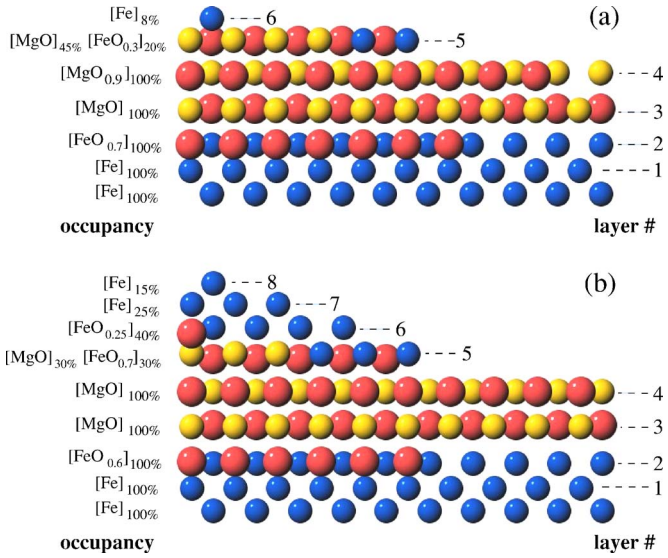

FIG. 5. (Color online) Model of the near-interface structure for samples grown by UHV method after deposition of 0.3 (a) and 7.8 (b). All symbols have the same meaning as in Fig. 3.

a few differences between the low-coverage (0.3 ML Fe) and high-coverage (7.8 ML) samples which are detailed below.

Up to 0.3 ML, all deposited Fe is in registry with the substrate lattice. We determine 0.2 ML Fe in the partially filled MgO layer (5) and 0.1 ML above the third-layer MgO islands (6). A small fraction of oxygen (≈10% of a monolayer) included in layer 5 improves the fit, leading to a $FeO_{0.3}$ stoichiometry in addition to 0.45 ML MgO. For the 7.8 ML sample a total amount of only 1.1 ML of Fe needs to be taken into account to optimize the fit quality, indicating that the majority of the deposited Fe (6.7 ML) is not in registry with the substrate lattice. There is some increased Fe concentration in the mixed (Mg, Fe) oxide layer (5) at the expense of Mg. Possibly some MgO is consumed by the formation of FeO. In the following three layers (6–8), only a small fractional occupancy of Fe is present, always well below 50%.

In correspondence with the chemical composition of the layers, inter layer distances are oxidelike (2.14 and 2.41 Å) for d_{45} and metal-like (1.4–1.7 Å) above.

On the basis of the structure models quite good agreement between experimental and calculated structure factor amplitudes could be achieved. We obtain R_u=7.9% and a GOF of 1.8 for the 0.3 ML sample and R_u=9.4% and a GOF of 1.7 for the 7.8 ML sample.

V. DISCUSSION

The analysis of the SXRD data indicates significant differences between the structures of the samples depending on whether Fe is initially deposited under ambient oxygen atmosphere or whether Fe is deposited solely under UHV conditions. In the latter case the majority of the deposited Fe (6.7 out of 7.8 ML) does not contribute to the scattered intensity. It is concluded that this fraction of the Fe film is not in registry with the underlying crystal lattice. By contrast, for

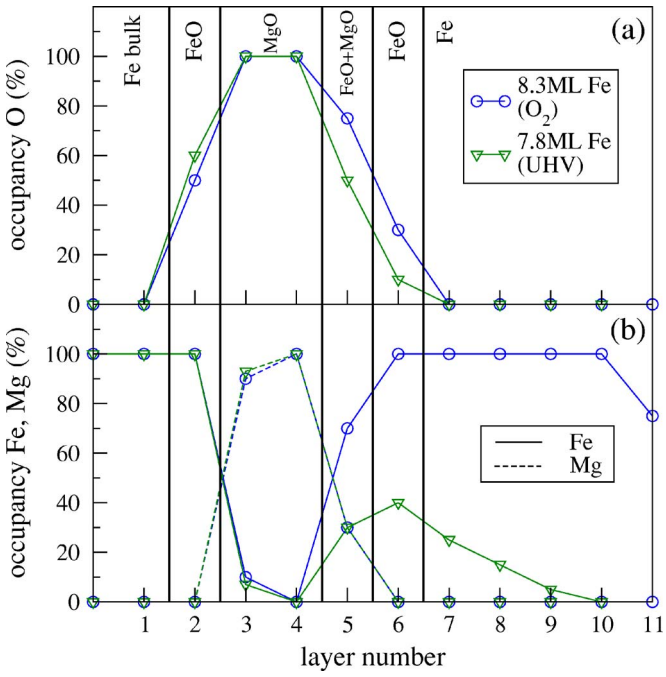

FIG. 6. (Color online) Layer-resolved concentration profile of oxygen (a), and iron and magnesium (b) for high-Fe-coverage samples grown under UHV-only (triangles) and oxygen-assisted (circles, squares) conditions. Solid and dashed lines in (b) represent Fe and Mg, respectively.

the oxygen-assisted deposition, a high degree of structural order is determined throughout the MTJ.

The different growth behavior and MTJ structure can be attributed to the formation of the FeO_x interface layer between the MgO spacer and the upper Fe electrode. Without presence of the FeO_x interface layer, subsequent growth of ordered Fe layers is not observed.

In order to emphasize the preparation dependence of the MTJ structure, the SXRD-derived concentration profiles are outlined in Fig. 6 on the basis of the high-coverage samples (8.3 and 7.8 ML). The upper (a) and lower (b) panel show the oxygen and metal occupancy versus layer number, respectively. At the top of the figure, the layers are labeled according to their gross chemical composition. Up to layer 4, i.e., the second complete MgO layer, the concentrations of the species in the two samples are very similar, indicating the remarkable reproducibility of the independent experimental results. There is only a 10% difference between the oxygen occupancies of the lower FeO_x layer (layer 2 with 50% versus 60%). This is about the upper limit of the uncertainty of the site occupancy determination.

Clear differences between the concentration profiles exist beginning with layer 5. There is an enhanced oxygen concentration within the Fe/MgO interface region (layers 5 and 6) for sample O_2 as compared to the UHV sample. Secondly, there is a remarkable difference between the fillings of the subsequent layers by Fe. One can quantitatively relate the coherent growth of the Fe layers to the presence of the interfacial FeO_x layer. In the case of UHV deposition, we find in layer 5 only a maximum of 30% of a ML of FeO_x above the complete MgO layer (4). The following layer (6) is occupied by a maximum only 40% of Fe in registry with the underlying lattice. In the case of oxygen-assisted growth, FeO_x fills the rest ($\approx$70%) of layer 5 as soon as more than 1.3 ML Fe are deposited (note that 30% of this layer is filled by MgO). Correspondingly, layer 6 is almost completely filled after deposition of 2.5 ML Fe [Fig. 3(c)].

From the thermodynamical point of view the dependence of the MTJ structure on the formation of the FeO_x layer can be attributed to the different interface contribution to the surface energy.[29] The interface contribution contains the specific chemical interaction between film and substrate, which is modified by the FeO_x interface layer. Using a qualitative crystallochemical approach we suggest that the interface layer leads to a reduction of the interface energy by allowing some fraction (50–70 %) of the Mg atoms at the interface to adopt the bulklike octahedral oxygen coordination. In contrast, without the FeO_x layer the Mg atoms would be left in a fivefold coordination located above Fe hollow sites. In summary, the FeO_x layer provides a "smoother" transition from the oxide barrier to the Fe film.

Finally, it should be noted that even in the case of UHV growth some FeO_x is present (the total amount of oxygen equals 0.31% of a monolayer in layers 5 and 6). With regard to the origin of the interface oxygen, no definite answer can be given. First, one could assume that oxygen comes from the residual gas atmosphere, but this appears to be an unlikely scenario, since even after several hours of measurements no oxidation of the surface Fe layers was observed. A more likely possibility is the reduction of adjacent MgO layers upon Fe deposition. Similar oxidation-reduction mechanisms were also observed for other transition metal/oxide interfaces such as in T/NiO(001), where T represents Fe, Co, or Ni.[30–32]

The lack of registry of the top Fe electrode in UHV samples might have considerable impact on the propagation of the Bloch states from the MgO spacer into the Fe electrode. This is because coherent tunneling conserving the electron's parallel momentum ($\vec{k}_{\parallel}$) is less probable in this case. Since the SXRD analysis involving the integer-order CTRs is highly sensitive to the lateral order of the adsorbate with respect to the (1×1) substrate cell, it exactly probes the fraction of the deposited film which contributes to coherent tunneling. Because in theoretical studies always coherent tunneling from the MgO spacer into the top electrode is assumed, the presence of a disordered top Fe layer might in part explain differences between theoretical and experimental TMR values. Furthermore, the coherent and symmetric MTJ structure can theoretically be related to higher TMR ratios as compared to those with a coherent but asymmetric interface structure with only one FeO_x layer.[33,34]

VI. SUMMARY

In summary, we have presented a detailed SXRD study of the structure and growth of the Fe/MgO/Fe(001) MTJ. Coherent growth of the top Fe electrode on the MgO barrier is achieved if an interface FeO_x layer ($x=0.6\pm0.1$) is prepared by depositing the first 0.5 ML of Fe in ambient oxygen ($p_{O_2}=10^{-7}$ mbar) atmosphere. This leads to a symmetric

MTJ structure characterized by two FeO_x layers: $Fe/FeO_x/MgO/FeO_x/Fe(001)$. By contrast, for deposition under UHV conditions, only a minor fraction ($\approx 30\%$ of a monolayer) of the FeO_x layer is observed at the upper interface. This is related to the absence of coherent growth of the subsequently deposited Fe film, leaving the top Fe electrode in a disordered structure relative to the underlying crystal lattice. Our results might have considerable implications for achieving giant TMR values which are a prerequisite for technological applications. The oxygen-assisted procedure described in this study could be the method of choice for future advances in the Fe/MgO/Fe(001) system.

ACKNOWLEDGMENTS

We would like to thank the ESRF for hospitality during our visit. Help by M. Noblet is also gratefully acknowledged. C.T. also acknowledges support by the Forschergruppe 404 of the German Science Foundation (DFG).

*Electronic address: tusche@mpi-halle.mpg.de

[1] M. Julliere, Phys. Lett. **54A**, 225 (1975).
[2] G. A. Prinz, Sci. Compass **282**, 1660 (1998).
[3] D. Wang, C. Nordman, J. M. Daughton, Z. Qian, and J. Fink, IEEE Trans. Magn. **40**, 2269 (2004).
[4] W. H. Butler, X.-G. Zhang, T. C. Schulthess, and J. M. MacLaren, Phys. Rev. B **63**, 054416 (2001).
[5] W. Wulfhekel, M. Klaua, D. Ullmann, F. Zavaliche, J. Kirschner, R. Urban, T. Monchesky, and B. Heinrich, Appl. Phys. Lett. **78**, 509 (2001).
[6] M. Klaua, D. Ullmann, J. Barthel, W. Wulfhekel, J. Kirschner, R. Urban, T. L. Monchesky, A. Enders, J. F. Cochran, and B. Heinrich, Phys. Rev. B **64**, 134411 (2001).
[7] J. Mathon and A. Umerski, Phys. Rev. B **63**, 220403(R) (2001).
[8] X.-G. Zhang, W. H. Butler, and A. Bandyopadhyay, Phys. Rev. B **68**, 092402 (2003).
[9] C. Tiusan, J. Faure-Vincent, C. Bellouard, M. Hehn, E. Jouguelet, and A. Schuhl, Phys. Rev. Lett. **93**, 106602 (2004).
[10] J. Faure-Vincent, C. Tiusan, E. Jouguelet, F. Canet, M. Sajieddine, C. Bellouard, E. Popova, M. Hehn, F. Montaigne, and A. Schuhl, Appl. Phys. Lett. **82**, 4507 (2003).
[11] S. Yuasa, A. Fukushima, T. Nagahama, K. Ando, and Y. Suzuki, Jpn. J. Appl. Phys., Part 2 **43**, L588 (2004).
[12] S. Yuasa, T. Nagahama, A. Fukushima, Y. Suzuki, and K. Ando, Nat. Mater. **3**, 868 (2004).
[13] H. L. Meyerheim, R. Popescu, J. Kirschner, N. Jedrecy, M. Sauvage-Simkin, R. Pinchaux, and B. Heinrich, Phys. Rev. Lett. **87**, 076102 (2001).
[14] H. L. Meyerheim, R. Popescu, N. Jedrecy, M. Vedpathak, M. Sauvage-Simkin, R. Pinchaux, B. Heinrich, and J. Kirschner, Phys. Rev. B **65**, 144433 (2002).
[15] B. D. Yu and J.-S. Kim, Phys. Rev. B **73**, 125408 (2006).
[16] J. L. Vassent, A. Marty, B. Gilles, and C. Chatillon, J. Cryst. Growth **219**, 434 (2000).
[17] L. Z. Mezey and J. Giber, Jpn. J. Appl. Phys., Part 1 **21**, 1569 (1982).
[18] S. H. Overbury, P. A. Bertrand, and G. A. Somorjai, Chem. Rev. (Washington, D.C.) **75**, 547 (1975).
[19] R. Hubert, J. Darville, and J. M. Gilles, Phys. Scr., T **4**, 179 (1983).
[20] G. Fahsold, A. Pucci, and K. H. Rieder, Phys. Rev. B **61**, 8475 (2000).
[21] B. M. Lairson, A. P. Payne, S. Brennan, N. M. Rensing, and B. J. Daniels, J. Appl. Phys. **78**, 4449 (1995).
[22] I. Robinson and D. J. Tweet, Rep. Prog. Phys. **55**, 599 (1992).
[23] R. Feidenhans'l, Surf. Sci. Rep. **10**, 105 (1989).
[24] J. Kirschner, H. Engelhard, and D. Hartung, Rev. Sci. Instrum. **73**, 3853 (2002), and references therein.
[25] I. K. Robinson, Phys. Rev. B **33**, 3830 (1986).
[26] E. Vlieg, J. Appl. Crystallogr. **30**, 532 (1997).
[27] The goodness of fit is defined as $\sqrt{\Sigma\sigma^{-2}(|F_{obs}|-|F_{calc}|)^2/(N-P)}$ and R_u is defined as $\Sigma\|F_{obs}|-|F_{calc}\|/\Sigma|F_{obs}|$, where σ is the standard deviation, P the number of free parameters, and F_{obs} and F_{calc} the observed and calculated structure factors, respectively; the summation runs over all N data points.
[28] S. C. Abrahams, Acta Crystallogr., Sect. A: Cryst. Phys., Diffr., Theor. Gen. Crystallogr. **25**, 165 (1969).
[29] E. Bauer and J. H. van der Merwe, Phys. Rev. B **33**, 3657 (1986).
[30] T. J. Regan, H. Ohldag, C. Stamm, F. Nolting, J. Lüning, J. Stöhr, and R. L. White, Phys. Rev. B **64**, 214422 (2001).
[31] R. de Masi, D. Reinicke, F. Müller, P. Steiner, and S. Hüfner, Surf. Sci. **515**, 523 (2002).
[32] C. Tusche, H. L. Meyerheim, F. U. Hillebrecht, and J. Kirschner, Phys. Rev. B **73**, 125401 (2006).
[33] C. Tusche, H. L. Meyerheim, N. Jedrecy, G. Renaud, A. Ernst, J. Henk, P. Bruno, and J. Kirschner, Phys. Rev. Lett. **95**, 176101 (2005).
[34] C. Tusche, H. L. Meyerheim, N. Jedrecy, G. Renaud, A. Ernst, J. Henk, P. Bruno, and J. Kirschner, Phys. Rev. Lett. **96**, 119602 (2006).